ANNUAL REVIEWS

Annual Review of Biomedical Engineering

Quantitative Molecular Positron Emission Tomography Imaging Using Advanced Deep Learning Techniques

Habib Zaidi[1,2,3,4] and Issam El Naqa[5,6,7]

[1]Division of Nuclear Medicine and Molecular Imaging, Geneva University Hospital, 1211 Geneva, Switzerland; email: habib.zaidi@hcuge.ch

[2]Geneva Neuroscience Centre, University of Geneva, 1205 Geneva, Switzerland

[3]Department of Nuclear Medicine and Molecular Imaging, University of Groningen, 9700 RB Groningen, Netherlands

[4]Department of Nuclear Medicine, University of Southern Denmark, DK-5000 Odense, Denmark

[5]Department of Machine Learning, Moffitt Cancer Center, Tampa, Florida 33612, USA

[6]Department of Radiation Oncology, University of Michigan, Ann Arbor, Michigan 48109, USA

[7]Department of Oncology, McGill University, Montreal, Quebec H3A 1G5, Canada

Annu. Rev. Biomed. Eng. 2021. 23:249–76

First published as a Review in Advance on April 2, 2021

The *Annual Review of Biomedical Engineering* is online at bioeng.annualreviews.org

https://doi.org/10.1146/annurev-bioeng-082420-020343

Keywords

artificial intelligence, machine learning, deep learning, molecular imaging, quantification

Abstract

The widespread availability of high-performance computing and the popularity of artificial intelligence (AI) with machine learning and deep learning (ML/DL) algorithms at the helm have stimulated the development of many applications involving the use of AI-based techniques in molecular imaging research. Applications reported in the literature encompass various areas, including innovative design concepts in positron emission tomography (PET) instrumentation, quantitative image reconstruction and analysis techniques, computer-aided detection and diagnosis, as well as modeling and prediction of outcomes. This review reflects the tremendous interest in quantitative molecular imaging using ML/DL techniques during the past decade, ranging from the basic principles of ML/DL techniques to the various steps required for obtaining quantitatively accurate PET data, including algorithms used to denoise or correct for physical degrading factors as well as to quantify tracer uptake and metabolic tumor volume for treatment monitoring or radiation therapy treatment planning and response prediction.

This review also addresses future opportunities and current challenges facing the adoption of ML/DL approaches and their role in multimodality imaging.

Contents

1. INTRODUCTION

Since the watershed year of 2012 and the subsequent success of deep learning (DL) algorithms, which outperformed other competing classification algorithms in the Google ImageNet database (1), there has been renewed interest in artificial intelligence (AI) and particularly DL for multimodality medical imaging applications (2–6). DL is a subcategory of machine learning (ML) techniques that allows for image data representation (e.g., feature extraction) and task learning (e.g., classification or detection) in the same framework. In other words, DL algorithms have the intrinsic ability to efficiently learn the relevant features of the task at hand directly from raw molecular imaging data, thereby saving valuable time and, more importantly, mitigating potential bias risks associated with human-crafted features and their selection process. However, DL comes with a need for more information and sufficient representative and annotated data sets compared with conventional ML approaches. The availability of large-scale annotated natural databases (e.g., ImageNet) has contributed to an additional pipeline of information for medical

image analysis through the process of transfer learning. In transfer learning, knowledge is carried from one domain to another to solve similar tasks. For instance, similar attributes (e.g., colors, edges, corners, textures) in natural images and medical images can contribute to the task of image segmentation or registration of molecular images. Through transfer learning, these tasks can be learned on the medical imaging domain with a smaller sample size by fine-tuning the algorithm to capture domain-specific salient features instead of learning the whole process from scratch. This capability is especially valuable in the case of molecular imaging, where information related to intensity differences, boundaries, edges, and possible textures is readily available from natural images and the DL/ML algorithms can focus on the salient features of physiological variations and tracer uptake distribution, for instance. Note that these technical advances in DL/ML developments and the tremendous growth in molecular imaging data sets have contributed to the potential deployment in the clinic of AI-based solutions, and specifically DL-based approaches, for solving molecular imaging challenges ranging from image analysis tasks (segmentation, registration, denoising, reconstruction, etc.) to improved diagnosis and prognosis (7, 8).

The bulk of AI research in the field to date has focused on positron emission tomography (PET) instrumentation design, image denoising (low-dose imaging), image reconstruction, quantification and segmentation, radiation dosimetry, and computer-aided diagnosis, as well as on finding a niche or primary clinical use. There has also been increased interest in the use of AI-based solutions in various applications to extract quantitative features (radiomics) from PET, including image segmentation and outcome prediction in clinical oncology. These novel techniques are revolutionizing clinical practice and are offering unique capabilities to the clinical molecular imaging community and biomedical researchers at large.

Previous reviews focused on DL-based medical image analysis in general (9–11) and DL-assisted quantitative PET imaging in particular (12, 13). This article discusses these topics and describes how AI and DL/ML are transforming the landscape of radiological sciences in general and molecular imaging in particular. It reviews state-of-the-art developments and the latest advances in DL-assisted quantitative molecular PET imaging developed to address the challenges associated with these techniques. It also presents an overview of potential promising developments and current and future clinical applications of these algorithms, as well as of the challenges facing the adoption of DL approaches in the clinic.

2. ADVANCES IN MOLECULAR IMAGING USING HYBRID TECHNOLOGIES

This is an exciting time for molecular imaging using PET technology, which is combined with either computed tomography (PET/CT) or magnetic resonance imaging (PET/MRI) to provide coregistered molecular and anatomical information. Although PET started mainly as a research tool for functional brain imaging (14), it became a widely used clinical tool, particularly in clinical oncology, following the advent of hybrid imaging (15). The combination of PET with CT was achieved by docking the two subsystems with minimal modification into a single gantry to acquire the two imaging modalities sequentially. The conceptual design of the CT scanners went through four generations to realize the modern geometries available today and their integration with PET scanners.

Technological advances in CT encompass innovative hardware and software developments, including single and dual X-ray tubes with higher output and faster rotation speeds, high-sensitivity detectors, dose-reduction strategies enabling faster scanning without sacrificing image quality, the ability to take advantage of sophisticated iterative reconstruction algorithms, and metal artifact reduction techniques (16). Likewise, PET instrumentation has undergone major technological

advances, including faster scintillation crystals with high stopping power combined with novel photodetector technologies to replace conventional bulky photomultiplier tubes (PMTs). These include solid-state technologies such as avalanche photodiodes (APDs) and, more recently, silicon photomultiplier tubes (SiPMs) operated in Geiger mode. Such MRI-compatible photodetectors can be easily operated within a magnetic field and as such are good candidates for building blocks of detector modules used in hybrid PET/MRI systems. Owing to their numerous advantages compared with PMTs, SiPMs have been implemented in modern digital PET scanners, which are now commercially available from major scanner manufacturers (17–19). Most of these scanners have a relatively large axial field of view, varying between 16.4 and 30 cm (20), yet they still cover only a portion of the body. In order to address this limitation, a high-sensitivity 194-cm-long total-body PET scanner was recently developed and is being characterized particularly in the context of dynamic whole-body imaging studies (21).

The availability of fast scintillators and readout technologies revived interest in the time-of-flight (TOF) technique, which enables enhanced localization of the annihilation position along the line of response through precise measurements of the difference between arrival times of the detected annihilation photons traveling at the speed of light. A substantial body of literature has demonstrated that TOF improves the signal-to-noise ratio in clinical studies, depending on the patient's size and the coincidence time resolution (CTR) of the scanner. Thus, TOF capability enables clinicians to reduce patients' injected dose and/or scanning time, increasing patient throughput. One manufacturer reduced the CTR on clinical PET systems from ~600 ps to ~214 ps (18), and it is expected that a CTR of 10 ps could be achieved within the next few years (22, 23). Such a low CTR would, in principle, obviate the need to perform image reconstruction since the physical limit of the spatial resolution for clinical scanners would be reached.

The widespread acceptance and success of PET/CT in clinical oncology triggered further research aiming to combine PET with MRI because of the latter's better soft tissue discrimination and multiparametric imaging capabilities. However, in contrast to PET/CT, combining PET with MRI without inducing mutual interference between the two subsystems is more technically challenging. The introduction of magnetic resonance–compatible photodetectors (APDs and SiPMs) facilitated this task, giving rise to different design concepts (24). Following the groundbreaking progress in preclinical PET/MRI instrumentation (25), various commercial and noncommercial clinical PET/MRI systems were developed during the last decade (26–32). **Table 1** presents the main characteristics of clinical PET/MRI systems used in both clinical and research settings.

Table 1 Main features of currently available clinical PET/MRI systems

System	Manufacturer	Operation	PET detector/ readout	Axial FOV	TOF	MRI	Reference
Ingenuity TF	Philips	Sequential	LYSO/PMTs	18 cm	Yes	3 T Achieva	26
Biograph mMR	Siemens	Simultaneous	LSO/APDs	25.8 cm	No	3 T Verio (modified)	27
SIGNA PET/MR	General Electric	Simultaneous	LYSO/SiPMs	25 cm	Yes	3 T MR 750w (modified)	28
Trimodality	General Electric	Sequential	LYSO/PMTs	15.7 cm	Yes	3 T MR 750w	29
BrainPET	Siemens	Simultaneous	LSO/APDs	19.2 cm	No	3 T Trio (modified)	30
uPMR 790	United Imaging Healthcare	Simultaneous	LYSO/SiPMs	32 cm	Yes	3 T uMR 790	32
Brain MGI	Academia	Sequential	LSO-LYSO/PMTs	25.2 cm	No	7 T Magnetom	31

Abbreviations: APD, avalanche photodiode; FOV, field of view; LSO, lutetium oxyorthosilicate; LYSO, lutetium yttrium oxyorthosilicate; MRI, magnetic resonance imaging; PET, positron emission tomography; PMT, photomultiplier tube; SiPM, silicon photomultiplier; TOF, time of flight.
Table adapted with permission from Reference 24.

PET/MRI technology appears to have reached maturity, but developments in instrumentation are still needed to optimize the conceptual design and simplify clinical procedures. Several challenges remain, however. To date, most PET/MRI methodological research has focused on tackling the intricacies of the quantitative imaging capabilities of this device owing to limitations in MRI-guided attenuation correction, particularly in whole-body imaging, in addition to establishing a primary clinical role for this modality to justify the additional investment cost.

3. CHALLENGES OF QUANTITATIVE MOLECULAR IMAGING BIOMARKERS

Since its inception, PET has demonstrated a solid foundation in terms of its ability to provide outstanding clinically relevant quantitative features. This has enabled the quantitative evaluation of molecular targets in a broad range of biochemical and physiological processes in vivo by establishing a correlation between the time-varying tracer uptake in organs/tissues and the kinetic parameters depicting the biological processes being assessed (33). Progress in PET instrumentation and imaging methodology has been significant and has paved the way toward faster scanning with enhanced sensitivity to reinforce the potential of translating PET's multiparametric quantitative imaging capabilities into the clinic. However, these quantitative imaging capabilities are challenged by several physical degrading factors that limit the potential of image-derived PET metrics in clinical and research settings, particularly in the context of monitoring response to treatment (34).

These physical factors involve mainly the physics of annihilation photons' interaction with the patient's body and the PET scanner's detectors/gantry as well as the performance of image reconstruction algorithms. Significant progress has been achieved in image reconstruction techniques, including iterative statistical algorithms with resolution recovery (35, 36). Photon attenuation and Compton scattering are among the main physical factors affecting the accuracy of PET quantification. These effects represent two sides of the same coin, in the sense that Compton scattering is the companion of attenuation because a considerable number of attenuated photons fall into the class of potential detected scattered events, provided that their energy falls within the defined energy acquisition window. The magnitude of these effects depends on the patient's size and the region of the body being scanned, and their correction requires a priori knowledge of the distribution of attenuation coefficients at 511 keV, referred to as the attenuation map, in the patient's body. Derivation of an attenuation map is relatively straightforward on hybrid PET/CT scanners, since CT measurements provide the required information about electron density. However, while MRI provides the anatomical information required for anatomo-functional mapping of disease on PET/MRI systems, in theory there is no direct correlation between the proton density of relaxation times and the electron density, making direct conversion of the MRI signal's intensity into a reliable attenuation map more challenging.

Despite innovative developments in PET instrumentation, the finite spatial resolution of whole-body clinical PET scanners remains a significant issue that affects small lesions' detectability and PET quantification accuracy. Therefore, small lesions occupy only part of the volume defined by the characteristic Gaussian representing the PET scanner's spatial resolution, defined as the full width at half-maximum. As a consequence, the recorded counts are spread over a larger volume covering neighboring regions, thereby blurring the lesion and underestimating its corresponding tracer uptake. The patient's bulk and cardiac/respiratory motion is another source of PET quantification bias that has been identified as an important degradation factor, particularly in the thoracic and upper abdomen regions, mainly at the level of the diaphragm. Therefore, nonnegligible errors might result from potential misalignment between the PET data and the

corresponding attenuation map acquired either sequentially or simultaneously on PET/CT or PET/MRI, respectively.

Static whole-body PET imaging provides only a snapshot of the tracer distribution averaged over a specific frame, limiting the analysis in clinical oncology to semiquantitative image-derived metrics, such as the standardized uptake value (SUV). In order to overcome this limitation, a promising approach involving the extraction of advanced radiomics has been developed, with the potential to provide consistent prognostic information with high predictive power in numerous malignant diseases (37, 38). Alternatively, dedicated protocols for whole-body dynamic imaging have been devised to enable the estimation of macro- or microkinetic parameters through graphical Patlak analysis or higher-order kinetic modeling techniques (39). These protocols have not only improved lesion detectability but also enhanced the quantitative capabilities of PET (40). AI and ML/DL may make significant contributions in all of these areas, as discussed in the next section.

4. OVERVIEW OF DEEP LEARNING APPROACHES AS APPLIED TO MEDICAL IMAGING AND MOLECULAR MEDICINE

As discussed above, DL constitutes a subcategory of ML that deals with representation learning, wherein raw information or images are fed directly into the algorithm and can automatically discover the underlying patterns (features) needed for the detection or classification tasks, as well as image quality enhancement, which are essential in the context of the lower image quality encountered in molecular imaging in comparison to other diagnostic imaging modalities, such as CT or MRI (41). Conceptually, this method of representation learning can be applied to any ML technology (**Figure 1**), but recent studies have shown that it is most effective with deep neural network (DNN) methods due to their universal approximation nature (42, 43). For completeness, below we briefly review the basic concepts of DNNs.

The basic building block of a neural network is the multilayer perceptron (MLP). A basic MLP, originally inspired by human neuron physiology, consists of three layers: an input layer, a hidden layer (or layers), and an output layer. The hidden layer (L) provides the nonlinear capability of the MLP and is generally characterized by a sigmoidal shape activation function (σ). Neural network architectures with more than two hidden layers are referred to as deep, hence the term deep learning. Given a data set of n samples (e.g., PET images) with inputs $\mathbf{x_i} \in R^m$, such as two-dimensional (2D) pixel or three-dimensional (3D) voxel intensities, and labeled outputs

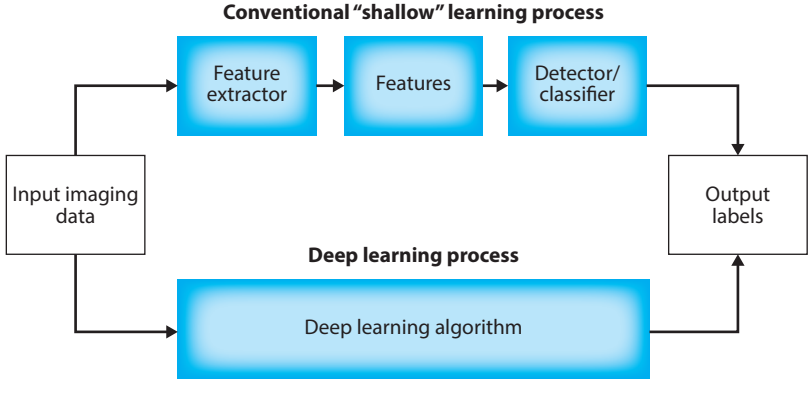

Figure 1

(*a*) Conventional "shallow" machine learning versus (*b*) deep learning algorithms, where image data representation and classification are handled within the same framework.

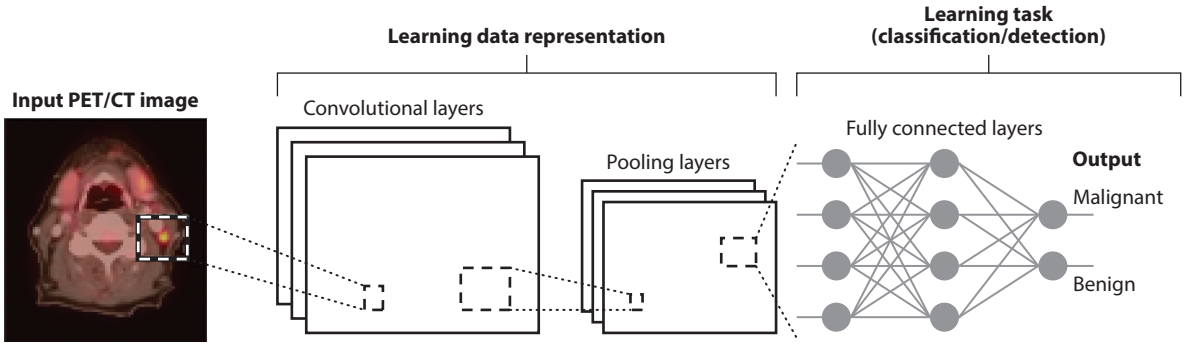

Figure 2

A convolutional neural network (CNN) architecture. A CNN consists of convolutional layers (filters) and pooling layers (data reduction operators) for data representation before the features are fed into a classifier (fully connected network). Abbreviation: PET/CT, positron emission tomography/computed tomography.

$y_i \in R$ (where $i = 1, \ldots, n$), such as PET image diagnostic status, an MLP with L layers input to output mapping can be represented by

$$f_{\mathbf{w},b}(\mathbf{x}) = \sigma_L\{\mathbf{w}^L \cdot \sigma_{L-1}[\mathbf{w}^{L-1} \cdots \sigma_1(\mathbf{w}^L \cdot \mathbf{x} + b^0) + b^{L-1}] + b^L\}, \quad 1.$$

where $\mathbf{w}^L$ are weight coefficients and b are biases estimated by minimizing a loss function, such as squared error or cross entropy, using gradient descent optimization with techniques such as the backpropagation algorithm. Choices of activation functions depend on the nature of the imaging data set and the task at hand (e.g., classification, detection, or regression); common ones include sigmoid, ReLu, eLu, and Leaky ReLU functions.

Among the best-known DL algorithms that have been widely applied in molecular imaging (see Section 5) are convolutional neural networks (CNNs) and their variants. An important characteristic of CNNs is their translation-invariant property, which is a main reason for their popularity in computer vision and molecular imaging applications. CNNs are biologically inspired by animals' visual cortex. In the 1990s, Lecun et al. (44) presented the first application of a CNN, LeNet, to read zip codes and digits. AlexNet, which won an ImageNet competition and spurred the current interest in medical imaging applications, is also a CNN architecture (1). A typical CNN (**Figure 2**) consists of several specialized layers, including convolutional and pooling layers (45). The convolutional layer, the main component of the network, applies an efficient filter (kernel) onto the image field (e.g., PET image voxels). In contrast, the fully connected layer has a somewhat tedious computational process, as in standard MLPs, aiming to capture and pass local information within a receptive field. The pooling layers perform data reduction with operations such as maximum or average pooling in order to achieve an efficient representation of the molecular image that can be more effectively related to the task, for instance, classification or detection of a lesion in a PET image.

Aside from CNNs and their variations such as the abovementioned LeNet and AlexNet, other neural networks such as Inception, VGG, ResNet, DenseNet, PyramidalNet, and U-Net have demonstrated improved classification and object recognition abilities in comparison to the original CNN in several medical applications, including PET imaging. These algorithms vary in their spatially invariant properties, depth and width, channel boosting, and attention mechanisms (46). Another type of DL algorithm that deals with data sequences and temporal information is the recurrent neural network (RNN). RNNs have had tremendous success in natural language processing (NLP), speech processing, genome-sequencing applications, and,

more recently, dynamic image analysis. Early RNNs suffered from optimization issues and were unable to process far-apart pieces of information. Modern RNNs are based on so-called long short-term memory (LSTM) architecture (e.g., transformer networks used in NLP). LSTM comprises basic units referred to as gates, which can learn to store and forget internal memory information and create long-term dependencies through a data sequence (47). Common gates include input, output, and forget gates, which tend to be computationally expensive. Therefore, researchers proposed a simplified architecture consisting of only two gates (reset and update), known as gated recurrent units (48). Another type of DL algorithm that has been widely applied in medical and molecular imaging is the generative adversarial network (GAN) (49). In GANs, two neural networks are pitted against each other in a zero-sum competition, one as a generator and the other as a discriminator. The generator tries to generate new data from random noise to mimic the real data, while the discriminator tries to distinguish any fake data from real data. This architecture has been successfully used for generating synthetic data (e.g., synthetic brain PET) and for transforming one imaging modality into another (e.g., MRI into synthetic CT or PET).

Many of the successful applications of DL in medical imaging are due to the role of transfer learning and data augmentation techniques in enriching and supplementing the limited medical and molecular imaging data available (50–53). For instance, AlexNet has been used to classify mediastinal lymph node metastasis in non-small-cell lung cancer from ^{18}F-FDG (fluorodeoxyglucose)-PET/CT images (54).

5. APPLICATIONS OF DEEP LEARNING IN QUANTITATIVE MOLECULAR IMAGING

Similar to other medical imaging modalities, DL methods have experienced tremendous growth and varying applications, ranging from PET instrumentation design and optimization to image reconstruction, quality, analysis, segmentation, and registration; dosimetry; computer-aided detection and diagnosis (CADe,x); and radiomics and outcome predictions (13). However, the use of DL in molecular imaging presents a distinct set of challenges in comparison to its sister conventional applications, arising from its goal of capturing biological processes and surrogate markers of disease pathophysiology as well as varying data structures and limited sizes (2), along with its role in diagnosis and treatment management as a functional modality that complements anatomical methods such as CT or MRI (55). **Table 2** presents a summary of these applications.

5.1. Positron Emission Tomography Instrumentation Design and Optimization

One application of DL in molecular imaging involves PET system design and optimization. In an early study, Wang et al. (56) used a conventional support vector machine to improve the spatial resolution of a preclinical PET scanner by classifying the primary fired pixels within the detector modules through Monte Carlo–based feature learning of positron trajectories. The proposed technique improved the spatial resolution in comparison to the energy-weighted centroid method. In contrast to the conventional detector-block design used in virtually all clinical PET scanners, monolithic crystals provide several advantages, including determination of the depth of interaction, but conventional positioning algorithms used to determine the interaction point pose a challenge. In this regard, the use of a DNN trained to predict the scintillation position using Monte Carlo simulation improved spatial resolution by approximately 18% with respect to conventional Anger logic without degrading sensitivity (57). Advances in TOF-PET technology have enabled the use of deep CNNs to estimate TOF directly from both digitized detector waveforms associated with a line of response (58). A simple experimental setup consisting of a moving positron-emitting point source and PMT-based detector modules demonstrated an

Table 2 Summary of deep learning applications in molecular PET imaging

Application	Algorithm or architecture	Reference(s)
Instrumentation design and optimization	DNN, CNN	57, 58, 148
Image reconstruction	DNN, CNN	55, 60–63
Attenuation and/or scatter correction and artifact reduction	DNN, CNN, encoder–decoder adversarial semantic structure, residual networks	64–74, 76–81
Segmentation	CNN, autoencoder, FCN, U-Net	88–91
Registration and motion correction	CNN, transformer	93, 94
Image quality improvement and denoising	DNN, CNN, GAN, cGAN, residual networks	95–108
Resolution enhancement	GAN	109
Internal radiation dosimetry	U-Net, DNN	113–115
CADe,x	CNN, Inception	116, 117
Radiomics	CNN, U-Net, DNN	118, 122–124

Abbreviations: CADe,x, computer-aided detection or diagnosis; cGAN, conditional generative adversarial network; CNN, convolutional neural network; DNN, deep neural network; FCN, fully convolutional network; GAN, generative adversarial network; PET, positron emission tomography.

improvement in TOF resolution of more than 20% in comparison to conventional techniques used in commercial systems, including leading-edge discrimination and constant fraction discrimination. Another interesting application of DL is the restoration of missing projection data owing to either defective detector blocks (59) or partial-ring geometries. Successful implementation of such approaches in total-body PET scanners should enable significant cost reduction, which would facilitate clinical adoption of this design concept.

5.2. Positron Emission Tomography Image Reconstruction, Quantification, Analysis, Segmentation, and Registration

Image analysis and processing are among the most direct applications of DL in molecular imaging and follow directly from their sister conventional applications in pattern recognition and computer vision. Image reconstruction from projections is an intuitive means of using DL to deal with the ill-posedness of the inverse reconstruction problem by enabling direct mapping of images from sinograms in an end-to-end manner (55, 60, 61). An alternative option is to incorporate the CNN directly into a statistical iterative reconstruction framework by expressing the objective function as a complex constrained optimization problem that can be worked out by using the alternating direction method of multipliers algorithm (62). A more elegant approach consists of incorporating DL into model-based iterative reconstruction in a maximum a posteriori (MAP) reconstruction approach by using a forward–backward splitting algorithm (63). Model-based DL reconstruction outperforms MAP and conventional postreconstruction DL-assisted denoising approaches (63).

Another area that has attracted considerable research interest is attenuation correction in hybrid imaging, particularly in PET/MRI, where MRI-guided attenuation correction is challenging owing to the lack of a direct relationship between (*a*) proton density and time-relaxation properties and (*b*) electron density (64). The complexity of the problem and the lack of a reliable and robust model based on imaging physics theory make the problem amenable to solution with DL algorithms. Several strategies employing various networks have been proposed to build a patient-specific DL-assisted attenuation map or pseudo-CT image derived from MRI (65–72). For example, **Figure 3** illustrates a patient's T_1-weighted MRI and reference CT images from a representative clinical study, along with attenuation maps derived by the commercial segmentation algorithm implemented in the Philips Ingenuity TF PET/MRI system, an Atlas-based approach (73), and a DL adversarial semantic structure algorithm (65). Similar techniques have

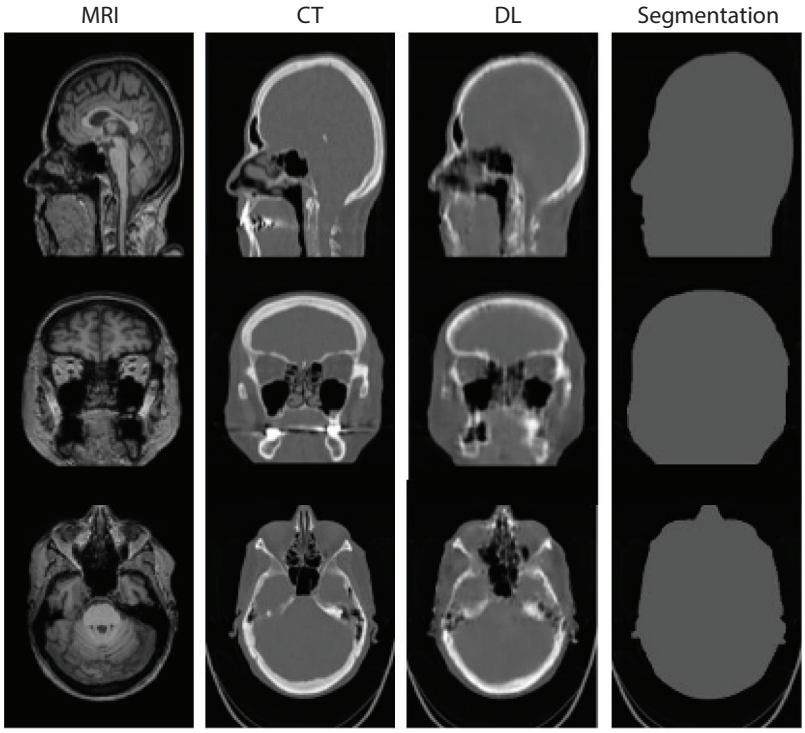

Figure 3

Comparison of three views of PET attenuation maps generated from MRI by use of a synthetic CT generation algorithm based on DL adversarial semantic structure of a representative clinical study. (*Left to right*) Target MRI, reference CT, DL-based attenuation map, and attenuation map of MRI segmentation into two tissue classes. Abbreviations: CT, computed tomography; DL, deep learning; MRI, magnetic resonance imaging; PET, positron emission tomography.

been employed to solve common problems encountered in PET/MRI, including truncation compensation and metal artifact reduction (74).

Advances in the field of theranostics have enabled the implementation of innovative approaches for the treatment of a plethora of systemic malignant diseases. However, quantitative imaging using radionuclides suitable for theranostic applications is inherently challenging owing to the complications associated with scatter correction (75). For example, a DL approach for scatter compensation in ^{90}Y bremsstrahlung single-photon emission computerized tomography (SPECT) imaging was proposed as an alternative to computationally intensive Monte Carlo–based simulations (76). DL-assisted joint correction for attenuation and scatter in an end-to-end fashion is another alternative approach that has recently been reported in several brain and whole-body PET studies (77–81).

Figure 4 illustrates the overall principle of DL-guided joint attenuation and scatter correction in PET. **Figure 5** depicts a representative clinical study comparing uncorrected PET; CT-based PET attenuation correction (PET-CTAC); and three variants of DL-based attenuation-corrected images, including 2D and 3D deep residual networks using 2D successive slices (PET-DL-2DS), 3D slices (PET-DL-3DS), and 3D patches (PET-DL-3DP), as well as difference SUV maps with respect to reference PET-CTAC images. The image quality of the DL-assisted joint attenuation and scatter correction framework is comparable to that of PET-CTAC. Quantification errors can

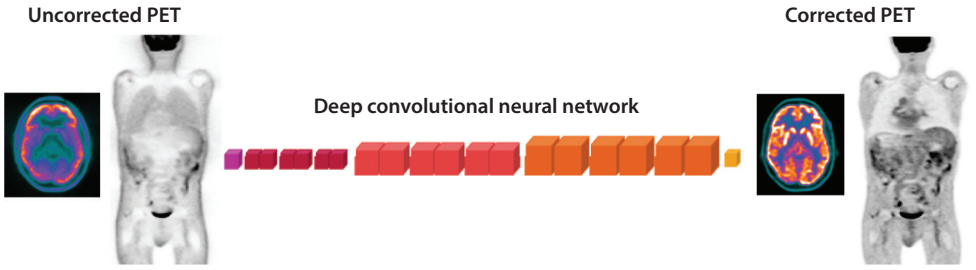

Figure 4

Principle of deep learning–assisted joint attenuation and scatter correction of PET images. The technique is feasible for both brain and whole-body PET imaging. Abbreviation: PET, positron emission tomography.

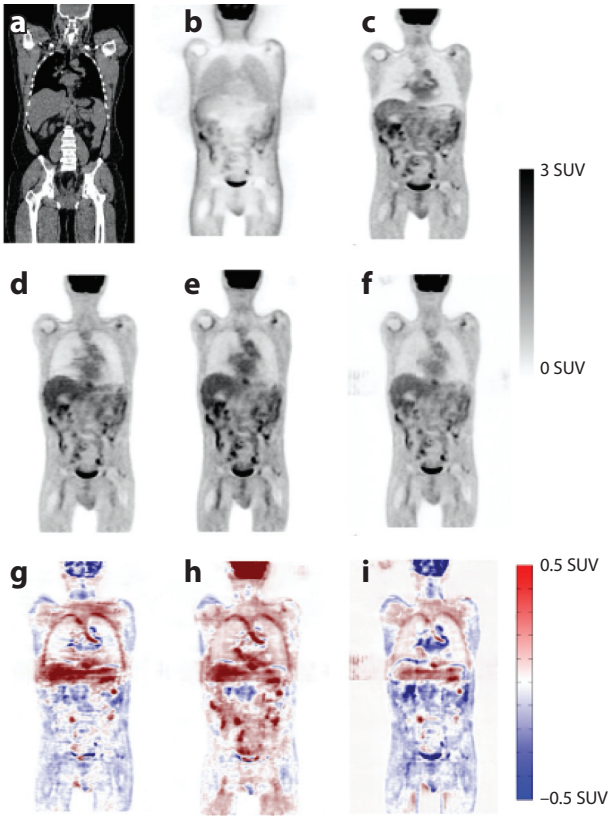

Figure 5

(*a–f*) Representative coronal views of PET images corrected for attenuation and scatter using DL-based approaches: (*a*) CT, (*b*) PET-CTAC, (*c*) uncorrected PET, (*d*) PET-DL-2DS, (*e*) PET-DL-3DS, and (*f*) PET-DL-3DP. (*g–i*) Difference bias maps for (*g*) PET-DL-2DS − PET-CTAC, (*h*) PET-DL-3DS − PET-CTAC, and (*i*) PET-DL-3DP − PET-CTAC. Abbreviations: CT, computed tomography; CTAC, CT-based PET attenuation correction; DL, deep learning; PET, positron emission tomography; PET-DL-2DS, DL-based deep residual networks using two-dimensional successive slices; PET-DL-3DP, DL-based deep residual networks using three-dimensional patches; PET-DL-3DS, DL-based deep residual networks using three-dimensional slices; SUV, standardized uptake value.

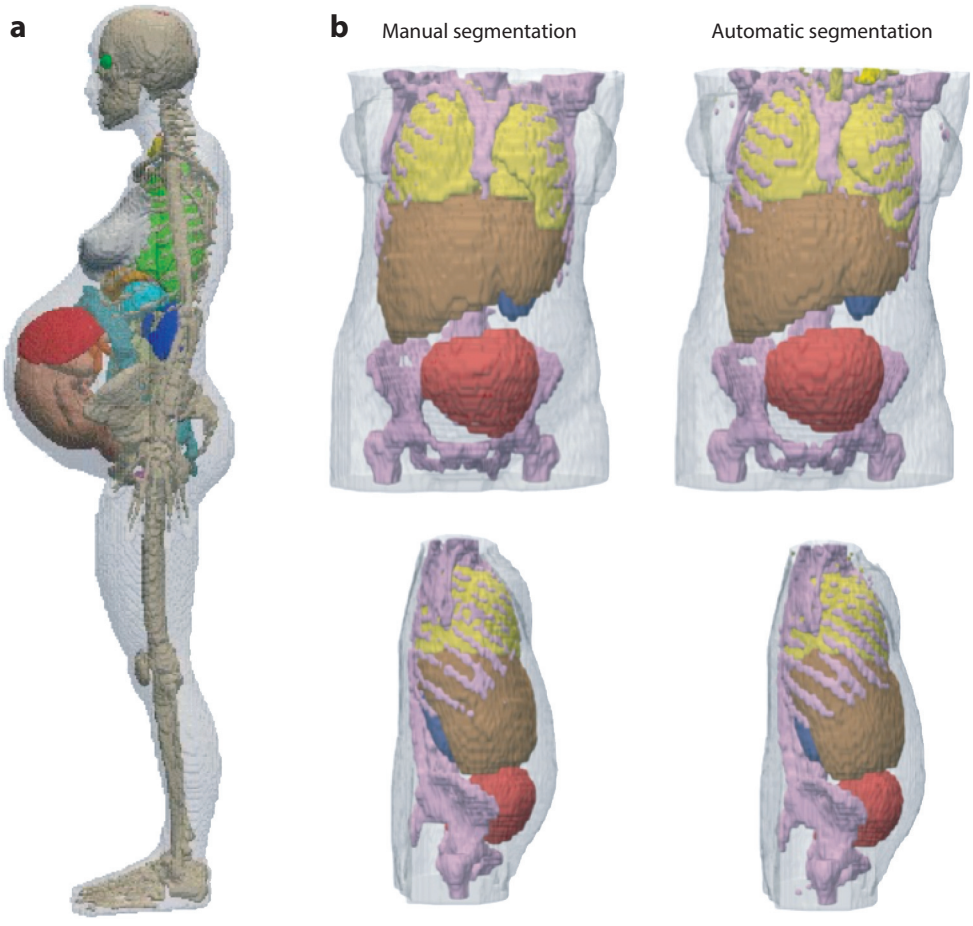

Figure 6

(*a*) Three-dimensional visualization of a computational pregnant female phantom at 38 weeks gestation; the uterus is rendered transparent to exhibit the fetus. (*b*) Three-dimensional views through representative slices of the computational model using (*left*) manual segmentation and (*right*) automated deep learning–based segmentation. The body is rendered transparent for enhanced display of internal organs and the skeleton.

be observed in the mediastinum and in regions with high heterogeneity and complexity, such as the liver, bones, soft tissues, and air cavities. Overall, the PET-DL-2DS algorithm provided better image quality and quantitative accuracy than the two 3D methods (80).

Segmentation is another classical problem in image analysis that has been comprehensively reviewed in the literature (82, 83). Image segmentation tasks that can be addressed using DL techniques include but are not limited to the development of computational anthropomorphic anatomical models for imaging physics and radiation dosimetry research (84) and segmentation of malignant lesions from PET images (85). A recent study reported an automated DL-guided algorithm for segmentation of CT images of pregnant female patients that was developed specifically for calculation of the radiation dose to the fetus from CT imaging procedures (86). **Figure 6** shows 3D coronal and sagittal views of this computational model, segmented using manually and DL-based segmentation techniques. Chen et al. (87) used a CNN with prior anatomical information to segment cervical PET images, achieving a Dice similarity coefficient (DSC) of

0.84. Li et al. (88) proposed a DL approach for variational multimodality tumor segmentation in lung cancer PET/CT in which they trained a fully convolutional network to produce a probability map from the CT image and then used a fuzzy variational model to incorporate the PET intensity probability map. The results for 84 PET/CT images yielded a DSC of 0.86. Blanc-Durand et al. (89) used 3D U-Net architecture for segmentation of ^{18}F-FET (fluoroethyltyrosine) PET in gliomas, achieving a DSC of 0.82 on testing. A large clinical database consisting of more than 1,300 PET images was used to train a 14-layer U-Net model with a pretrained encoder (90). More recently, a 20-layer residual CNN (HighResNet) algorithm was adopted for PET image segmentation (91). This algorithm achieved automated contour delineation with a DSC of 0.87 ± 0.04, exhibiting a promising performance for automated delineation of treatment volumes from head and neck PET images.

DL-guided image registration is another interesting application that has recently received considerable attention. A recent survey of 150 articles published during the last 3–4 years classified the various strategies into seven nonexclusive categories according to technique, functions, and popularity (92): (*a*) reinforcement learning–based methods, (*b*) deep similarity–based methods, (*c*) supervised transformation prediction, (*d*) unsupervised transformation prediction, (*e*) GANs for medical image registration, (*f*) registration validation using DL, and (*g*) other learning-based methods. An example is the unsupervised affine and deformable image registration framework implemented by stacking multiple CNNs into a larger network to carry out coarse-to-fine image registration (93). The algorithm achieved a performance similar to that of conventional deformable image registration and had the advantage of being computationally faster by several orders of magnitude.

Li et al. (94) used unsupervised DL for motion correction of respiratory-gated PET images within a nonrigid image registration framework. Their approach yielded a normalized root-mean-square error of $24.3 \pm 1.7\%$ compared with $31.1 \pm 1.4\%$ for the iterative registration-based motion correction and $41.9 \pm 2.0\%$ for ungated reconstruction (**Figure 7**).

5.3. Positron Emission Tomography Image Enhancement (Denoising, Low-Dose Scanning, Superresolution)

The use of DL techniques in superresolution, image denoising, and generation of high-quality from low-quality images has been at the forefront of applications in PET imaging. These techniques have been successfully employed for the generation of standard-dose PET images from low-dose scans both without (95, 96) and with (97) the exploitation of concurrent multiparametric anatomical magnetic resonance images for amyloid brain PET imaging. These techniques were implemented mostly in image space applied in PET imaging of partial body regions, including the brain, chest, abdomen, and pelvis (98, 99). Alternatively, the training of the data sets can be implemented in projection space, as reported by Sanaat et al. (100). **Figure 8** depicts transverse, coronal, and sagittal views illustrating reference full-dose, low-dose, and predicted full-dose PET images generated using the DL algorithm implemented in image space and projection space. A qualitative assessment by experienced observers revealed that the PET images generated from training in projection space outperformed those derived from implementation in image space in terms of quality and replication of ^{18}F-FDG uptake patterns (100).

Similar techniques using various networks have also been reported for ^{18}F-FDG whole-body PET imaging (101–106) and cardiac SPECT imaging (107, 108). These techniques enabled a substantial decrease in acquisition time in oncological and myocardial perfusion studies, respectively.

Another model focusing on resolution enhancement was presented by Song et al. (109), who used a dual GAN to generate superresolution brain PET images. The performance of this technique was significantly better than that of classical penalized deconvolution techniques, both qualitatively and quantitatively.

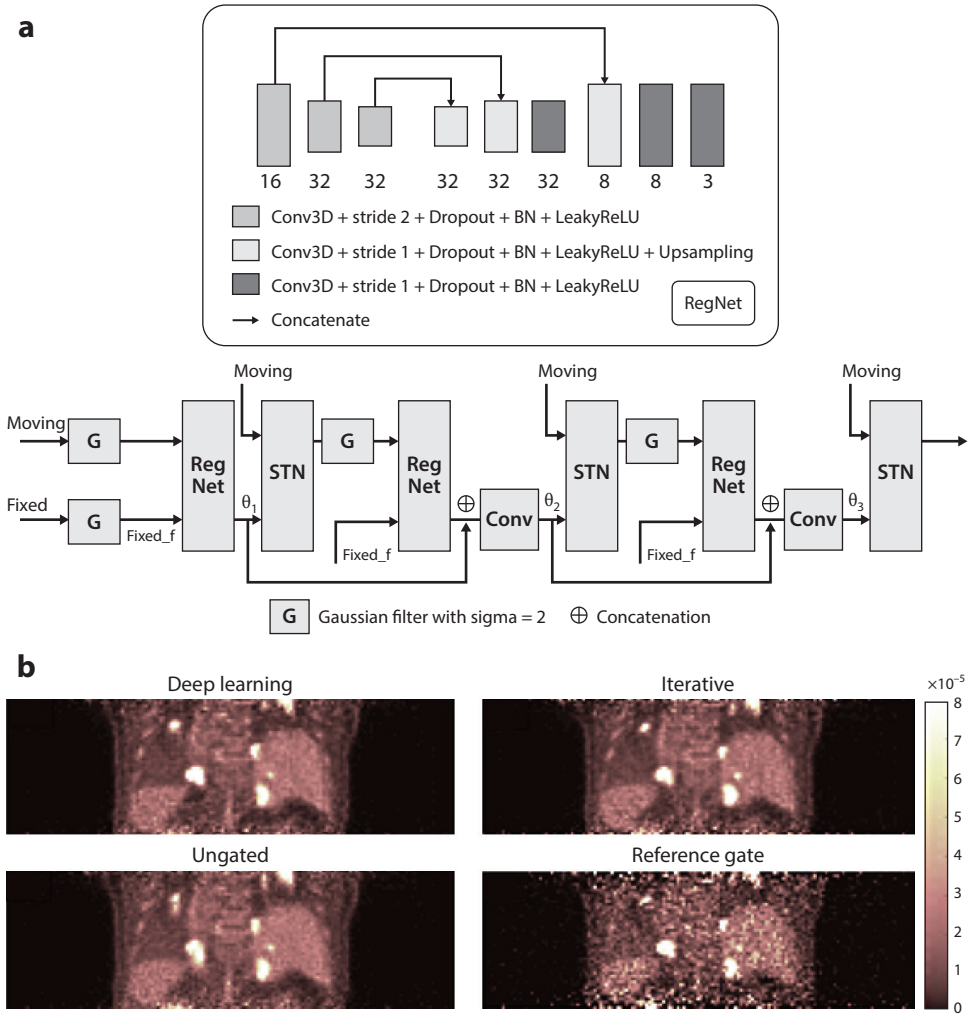

Figure 7

(*a*) Structure of the unsupervised deep learning registration network. (*b*) Sample results with different methods. Figure adapted with permission from Reference 94.

5.4. Radiation Dosimetry Calculations (Therapy Planning)

The use of DL algorithms in absorbed-dose calculations has been demonstrated in the case of external radiotherapy (110, 111) and brachytherapy (112), primarily to improve the efficiency of dose calculation while maintaining the same accuracy of traditional absorbed-dose calculation methods. In a study that applied DL to internal dosimetry (113), a U-Net-based dose rate map agreed well with the ground truth generated by Monte Carlo, with a voxel dose rate error of $2.54 \pm 2.09\%$. The performance of this approach was superior to that of the voxel S-value kernel convolution method, which achieved errors of $9.97 \pm 1.79\%$. A hybrid approach combining DL with empirical mode decomposition techniques used patients' density maps and medical internal radiation dosimetry (MIRD) organ S-value-derived dose maps and cumulated activities estimated

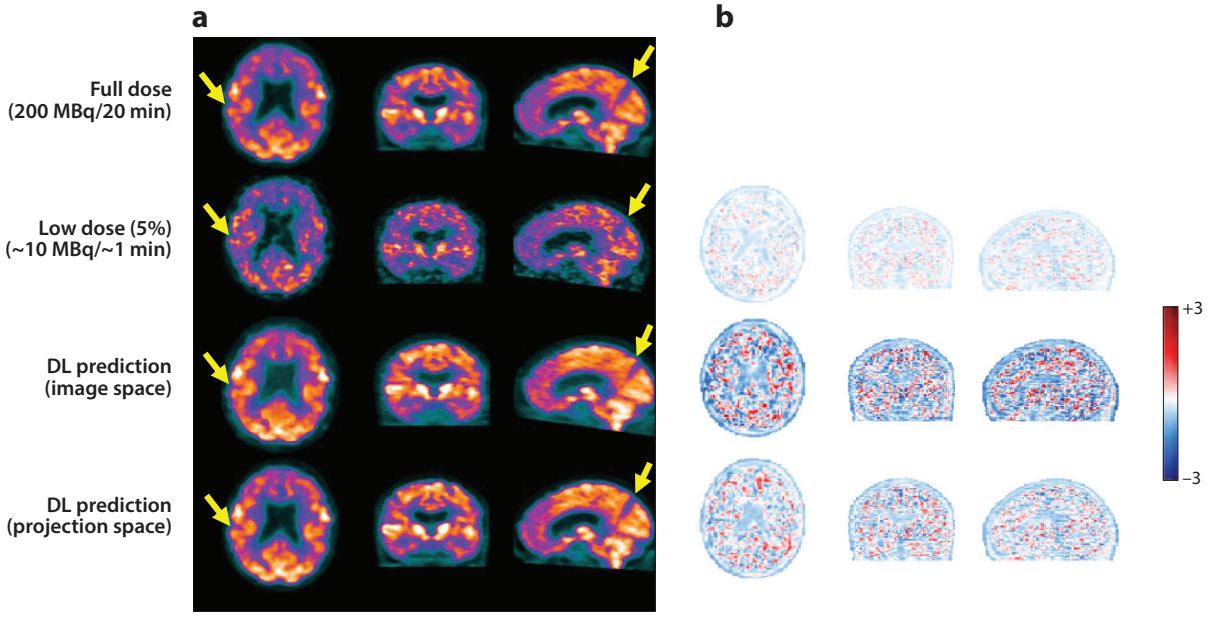

Figure 8

Representative ^{18}F-FDG brain PET images. (*a*) Reference full-dose images and the corresponding low-dose and predicted full-dose images in the image and sinogram space. (*b*) SUV bias maps for low-dose, PIS, and PSS PET images with respect to the reference full-dose PET image. Abbreviations: DL, deep learning; FDG, fluorodeoxyglucose; PET, positron emission tomography; PIS, prediction in image space; PSS, prediction in projection space; SUV, standardized uptake value.

from ^{177}Lu SPECT images to predict patient-specific absorbed-dose distributions (114). Similarly to the first approach, this network was trained using Monte Carlo simulations.

More recently, researchers developed a DL-based approach that enables prediction of patient-specific, whole-body, organ-level dosimetry accounting for heterogeneous time-varying tracer uptake and nonuniform distribution of the attenuation medium (115). **Figure 9** illustrates the basic principle of this approach. In essence, the algorithm expands the well-established voxel-based MIRD formalism to build a 3D dose map from a single S-value kernel to personalized S-value kernels by using patient-specific PET/CT images. The DNN is trained using CT images to derive the corresponding density maps and Monte Carlo–generated voxelwise S-values. Consequently, the trained model and whole-body dose maps obtained by convolving specific voxel S-values with the activity map are used to infer specific S-value kernels. The technique appears suitable for whole-body internal dosimetry, as its performance is similar to that of direct Monte Carlo simulations and it addresses the drawbacks of conventional techniques.

5.5. Computer-Aided Detection and Diagnosis

Computer-aided detection (CADe) and computer-aided diagnosis (CADx) were among the earliest applications of AI and ML/DL and flourished in the 1980s and 1990s. A recent review article traces the history of AI in radiology to modern applications (11). Many of these CADe,x applications focused on anatomical imaging, particularly in the breast (mammography) and in the lung; they played less of a role in molecular imaging or PET, probably due to limited volume on one hand and the complexity of quantitative interpretation of PET images compared with anatomical ones on the other hand. The emergence of DL has provided new opportunities to

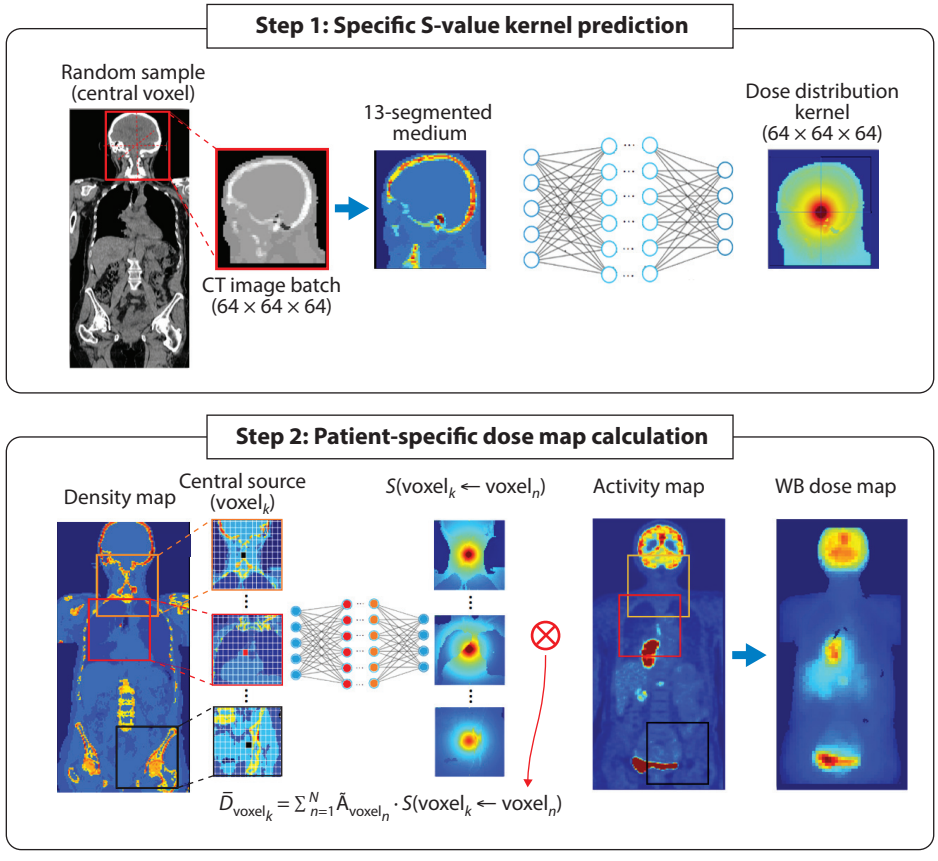

Figure 9

Schematic representation of the voxel-scale dosimetry procedure. Steps 1 and 2 illustrate the deep learning–based specific S-value kernel prediction and MIRD-based voxel dosimetry formalism, respectively. Abbreviations: CT, computed tomography; MIRD, medical internal radiation dosimetry; WB, whole-body. Figure adapted with permission from Reference 115.

reexamine CAD in molecular imaging. In a CADx application, Ding et al. (116) developed a DL algorithm to predict Alzheimer disease by using FDG-PET of the brain. The DL algorithm is based on the Inception CNN transfer learning architecture, which was pretrained on ImageNet and fine-tuned using 90% of the Alzheimer disease data set. The algorithm achieved an area under the curve of 0.98 (95% CI, 0.94–1.00) on the remaining 10%. Model interpretability was performed using feature saliency maps and t-SNE (t-distributed stochastic neighbor embedding) clustering plots. In a CADe,x application, Sibille et al. (117) examined several CNN configurations for localization and classification of FDG-PET uptake patterns in patients with lung cancer and lymphoma. They found that performance improved when both CT and PET images were used in comparison to either alone. **Figure 10** depicts the CADe,x pipeline and sample results.

5.6. Radiomics and Outcome Prediction Models

Radiomics is an image analytics field that involves extracting large numbers of imaging features that can be related to biological and clinical endpoints (e.g., imaging biomarkers), with several

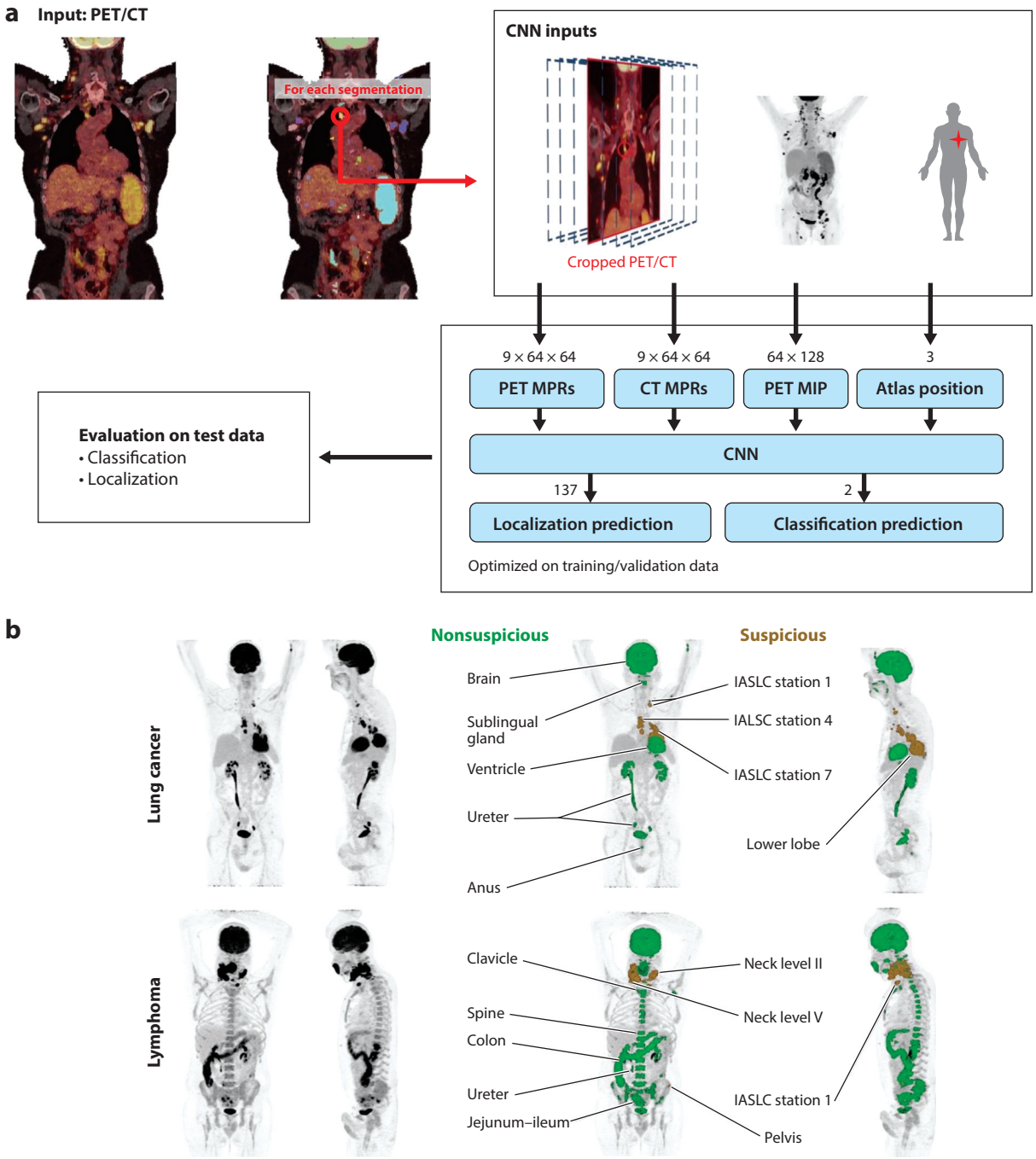

Figure 10

(*a*) Pipeline developed with a CNN for PET CADe,x. (*b*) MIP ^{18}F-FDG-PET/CT images from two patients, processed by the CNN. The patients with lung cancer and lymphoma are from the test data set; areas of uptake were automatically color-coded by their classification and localization. Abbreviations: CADe,x, computer-aided detection and diagnosis; CNN, convolutional neural network; CT, computed tomography; FDG, fluorodeoxyglucose; IASLC, International Association for the Study of Lung Cancer; MIP, maximum intensity projection; MPR, multiplanar reformation; PET, positron emission tomography.

academic and commercial platforms devoted to its analytics (118). PET radiomics was one of the earliest imaging modalities used for this purpose, particularly for applications in oncology (119). Conventional radiomics relies on the combination of human-engineered features, such as shapes and textures that are based on computer vision and pattern recognition methodologies, with statistical learning or ML tools to build predictive or prognostic models (120, 121). In contrast, more modern radiomics applications have shifted toward utilizing DL for data representation rather than handcrafting approaches (122). Given current sample size limitations, the trend in both single and multiple imaging modalities has been to combine human-engineered features with DL features to achieve the best performance (123, 124), where expert prior knowledge can substitute for insufficient representative data samples. These two frameworks of radiomics are reviewed in Reference 118 and depicted in **Figure 11**.

6. ISSUES WITH MEDICAL IMAGING CHALLENGES AND RANKINGS OF COMPETITIONS

The AI and ML/DL community has witnessed groundbreaking algorithmic developments, and many of the algorithms are available to end users and developers as open-source software that can be further evaluated and validated for potential deployment in clinical and research settings. However, as reported by Hutson (125), only a small fraction of AI research papers provide code or pseudocode, which is prejudicial to reproducible research (126). Leading professional societies [e.g., MICCAI Society, Radiological Society of North America, American Association of Physicists in Medicine, Society of Nuclear Medicine and Molecular Imaging (SNMMI)] often organize international challenges for validation and comparison of competitive medical image analysis algorithms, leading to the creation of rankings and guidelines regarding the performance of these approaches under controlled conditions by using public image repositories (127). Several of these challenges were set up to tackle major issues facing quantitative PET imaging, including MICCAI Society challenges on PET image segmentation (128, 129) and PET radiomics analysis (130), and the most recent SNMMI challenge on ^{177}Lu dosimetry based on quantitative SPECT imaging (131).

Despite the popularity of these challenges, which are viewed as a forum for scientists to demonstrate their inventive AI and ML/DL algorithms, their practical relevance and critical role are subject to debate (132). Criticisms raised in a detailed report evaluating 150 biomedical image analysis challenges performed prior to the end of 2016 include irregularities in quality, assessment, reproducibility, and ranking (133), which might jeopardize the outcome of these challenges and its reliability. The report identifies 53 parameters reflecting consistency in organizing, designing, and implementing challenges, with the aim of enhancing their planning in a well-thought-out manner. Incorporating these improvements by taking advantage of advanced cloud computing tools (134) and using modern tools to share confidential biomedical data (135) is anticipated to raise the profile of future challenges and bring them to the level required to interpret their outcomes with more confidence.

7. CURRENT LIMITATIONS AND CHALLENGES WITH DEEP LEARNING IN MOLECULAR IMAGING

The application of ML/DL in medical imaging in general and molecular imaging in particular is not without challenges or controversies. These include the scarcity of high-quality annotated data and mismatches between the development data set and the targeted environment for application (11), in addition to the causality between imaging features and clinical or biological endpoints (136). Details on general DL medical image analysis can be found in Reference 10.

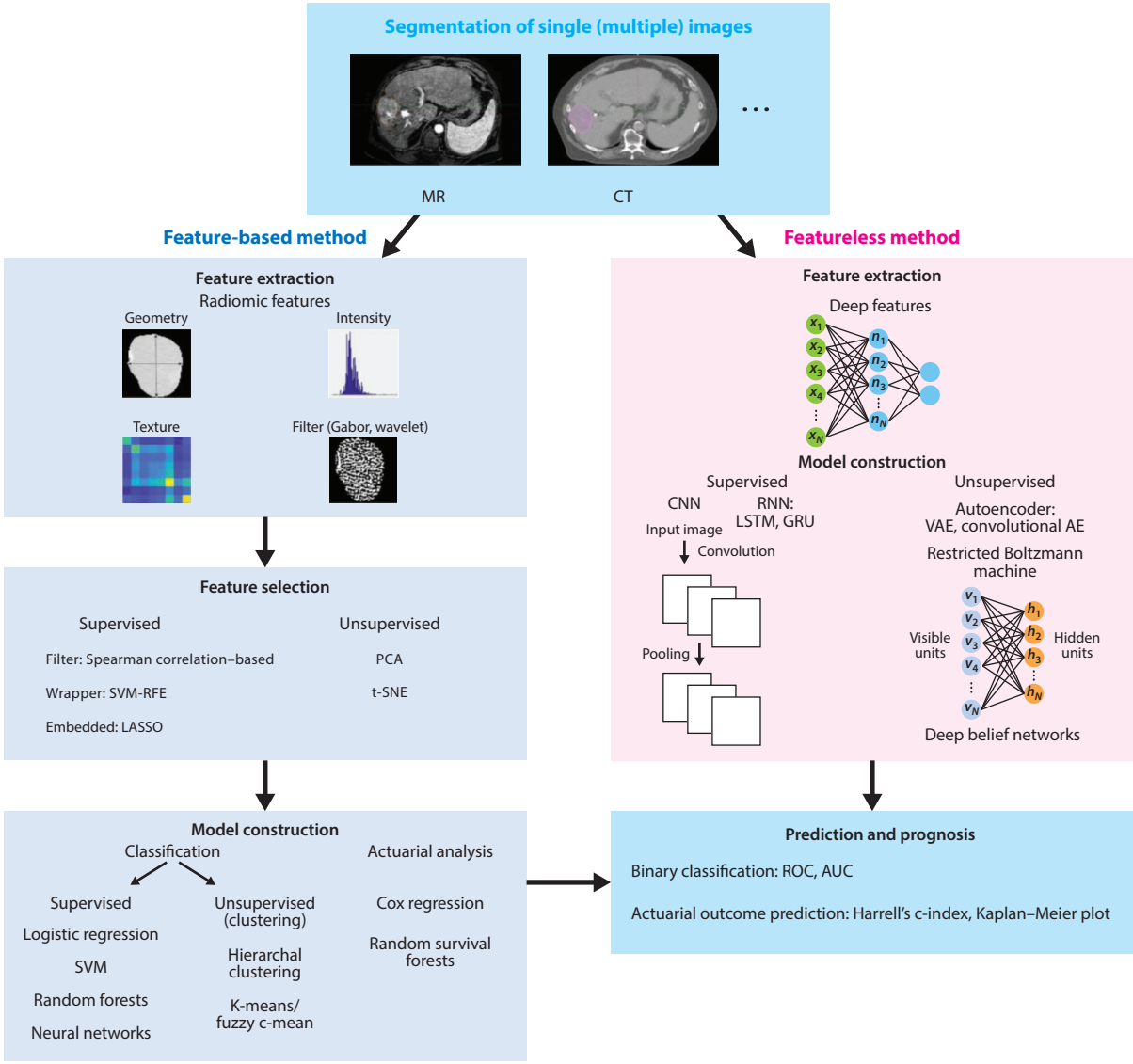

Figure 11

Workflow for radiomics analysis with feature-based (conventional machine learning) and featureless (deep learning) approaches. Abbreviations: AE, autoencoder; AUC, area under the curve; CNN, convolutional neural network; CT, computed tomography; GRU, gated recurrent unit; LASSO, least absolute shrinkage and selection operator; LSTM, long short-term memory; MR, magnetic resonance; PCA, principal component analysis; RFE, recursive feature elimination; RNN, recurrent neural network; ROC, receiver operating characteristic; SVM, support vector machine; t-SNE, t-distributed stochastic neighbor embedding; VAE, variational autoencoder.

7.1. Sample Size Requirements

Identifying the required sample size for training is key for building a successful ML or DL algorithm for a particular molecular imaging application. In order for the algorithm to generalize and succeed on out-of-sample data, it has to learn the current context properly, whether with labeled

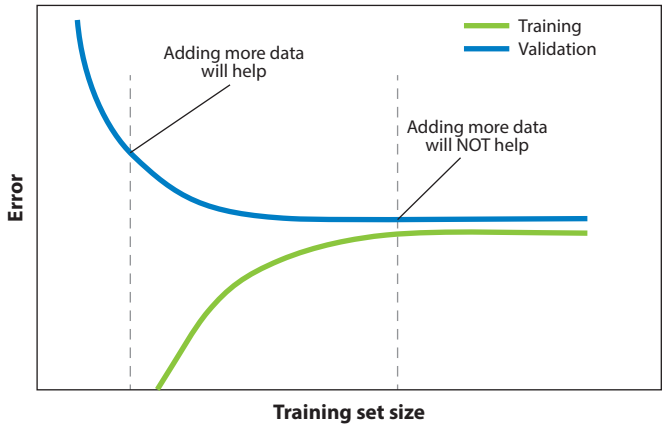

Figure 12

An example of a learning curve for analyzing the data size requirements for machine learning/deep learning development.

data (supervised learning) or without labels (unsupervised learning), or anything in between (semisupervised learning). These sample size requirements generally increase from conventional ML to DL algorithms; in the latter, both the data representation and the task need to be learned in the same framework. Unlike in traditional statistics, where power analysis tools are readily available to conduct the design a priori, such tools are scarce in ML/DL. Alternatively, learning curve (LC) techniques can be applied to the existing data to determine whether the sample is sufficient to meet the training requirements of the ML or DL algorithm at hand. Empirically, the more complex the problem/learning algorithm (e.g., the larger the number of free parameters) is, the more data will naturally be required (137). LC is an empirical graphical tool that can be used to evaluate whether there are sufficient samples for proper training. The idea is to first split the data set into three groups—training, validation, and testing—and then make a plot of a model performance metric for training and validation separately as a function of the number of the samples before evaluating its generalizability on the testing data. Plateauing of the performance metric (e.g., prediction error) on the training and validation sets indicates a sufficient sample size (**Figure 12**). In practice, it may be prudent to have more training and validation samples, as long as they are not too noisy. However, if collecting more molecular imaging data becomes infeasible, one can perform data augmentation or apply the transfer learning approaches discussed above (137).

7.2. Testing and Evaluation

As noted above, for an ML/DL algorithm to be practically useful, it must be able to generalize beyond the training and validation data sets into out-of-sample (testing) data. This capability can be evaluated by using resampling methods (cross-validation or bootstrapping) or bias–variance tradeoffs (Cramér–Rao), or analytically by using complexity measures such as the Vapnik–Chervonenkis dimension (138). External validation of models in cohorts acquired independently from the discovery cohort (e.g., from another radiology department) is still considered the gold standard for true estimates of performance and generalizability of prediction models (139).

Although several efforts to provide guidelines for developing and reporting ML/DL results are ongoing, the TRIPOD (transparent reporting of a multivariable prediction model for individual

prognosis or diagnosis) statement remains the most widely adopted (140). TRIPOD is a multitier validation process, ranging from internal to external and meta-analytical validations.

7.3. Model Interpretability

Clinical implementation and utilization of ML/DL will require an improved ability to interpret ML/DL model findings. This may vary with the nature of the application; for instance, an improvement in image quality or good segmentation can be easily judged by observing the results. However, in the case of outcome modeling (e.g., radiomics), it cannot be easily judged; therefore, interpretation of the features would lead to better understanding and provide more trust in the model performance. There exist many approaches to achieve this interpretability goal, ranging from the design of the algorithm to post hoc analyses (141). In the context of DL, approaches include deriving proxy models, developing attention maps, and providing disentangled representation or learning with known operators to create a more interpretable ML/DL framework (142–146).

8. CONCLUSIONS AND FUTURE DIRECTIONS

The past decade witnessed tremendous interest in the application of advanced data analytics to quantitative molecular imaging. This research interest has focused specifically on the role of ML/DL techniques and their potential to transform the landscape of molecular imaging and overcome many of its challenges. This review has presented examples of ML/DL in PET images and discussed the areas of instrumentation design and optimization, reconstruction, segmentation and registration, image quality, CAD, treatment planning, and outcome prediction. In each case, ML/DL techniques have demonstrated a performance comparable to or better than state-of-the-art approaches. However, despite this initial success, it is expected that these algorithms still have more to offer, especially in bridging the gap between technology development and implementation in clinical care. Challenges facing AI-guided PET imaging include the availability of high-quality annotated data, rigorous validation and testing to ensure reproducibility, and new tools to improve data interpretability in research and clinical practice. In any case, these novel techniques are revolutionizing current clinical practice and offering new, unique capabilities that will allow the molecular imaging community to meet its long-held goals of interrogating disease and personalizing treatment.

It is clear that a new generation of quantitative PET imaging tools is likely to further broaden the use of PET for radiological diagnosis, treatment management, and prognosis. However, large curated and annotated data sets for training and validation will be needed in order to fulfill the potential of AI and especially DL algorithms for better molecular imaging, which may require collaborations among multiple stakeholders and leading societies in the field. Although this review has focused on PET imaging, the same is true for SPECT and for other molecular imaging and theranostic techniques as well (147).

DISCLOSURE STATEMENT

The authors are not aware of any affiliations, memberships, funding, or financial holdings that might be perceived as affecting the objectivity of this review.

ACKNOWLEDGMENTS

The writing of this review was supported by the Swiss National Science Foundation (grant SNRF 320030_176052), the Eurostars Programme of the European Commission (grant E!12326

ILLUMINUS), the Private Foundation of Geneva University Hospitals (grant RC-06-01), and the US National Institutes of Health (grants R37-CA222215 and R01-CA233487).

LITERATURE CITED

1. Krizhevsky A, Sutskever I, Hinton GE. 2017. ImageNet classification with deep convolutional neural networks. *Commun. ACM* 60:84–90
2. Choi H. 2018. Deep learning in nuclear medicine and molecular imaging: current perspectives and future directions. *Nucl. Med. Mol. Imaging* 52:109–18
3. Giger ML. 2018. Machine learning in medical imaging. *J. Am. Coll. Radiol.* 15:512–20
4. Hosny A, Parmar C, Quackenbush J, Schwartz LH, Aerts H. 2018. Artificial intelligence in radiology. *Nat. Rev. Cancer* 18:500–10
5. Liu S, Wang Y, Yang X, Lei B, Liu L, et al. 2019. Deep learning in medical ultrasound analysis: a review. *Engineering* 5:261–75
6. Lundervold AS, Lundervold A. 2019. An overview of deep learning in medical imaging focusing on MRI. *Z. Med. Phys.* 29:102–27
7. Langlotz CP, Allen B, Erickson BJ, Kalpathy-Cramer J, Bigelow K, et al. 2019. A roadmap for foundational research on artificial intelligence in medical imaging: from the 2018 NIH/RSNA/ACR/The Academy workshop. *Radiology* 291:190613
8. Sahiner B, Pezeshk A, Hadjiiski LM, Wang X, Drukker K, et al. 2019. Deep learning in medical imaging and radiation therapy. *Med. Phys.* 46:e1–36
9. Litjens G, Kooi T, Bejnordi BE, Setio AAA, Ciompi F, et al. 2017. A survey on deep learning in medical image analysis. *Med. Image Anal.* 42:60–88
10. Shen D, Wu G, Suk HI. 2017. Deep learning in medical image analysis. *Annu. Rev. Biomed. Eng.* 19:221–48
11. El Naqa I, Haider MA, Giger ML, Ten Haken RK. 2020. Artificial intelligence: reshaping the practice of radiological sciences in the 21st century. *Br. J. Radiol.* 93:20190855
12. Wang T, Lei Y, Fu Y, Curran WJ, Liu T, et al. 2020. Machine learning in quantitative PET: a review of attenuation correction and low-count image reconstruction methods. *Phys. Med.* 76:294–306
13. Arabi H, Zaidi H. 2020. Applications of artificial intelligence and deep learning in molecular imaging and radiotherapy. *Eur. J. Hybrid Imaging* 4:17
14. Hooker JM, Carson RE. 2019. Human positron emission tomography neuroimaging. *Annu. Rev. Biomed. Eng.* 21:551–81
15. Jones T, Townsend D. 2017. History and future technical innovation in positron emission tomography. *J. Med. Imaging* 4:011013
16. Lell MM, Wildberger JE, Alkadhi H, Damilakis J, Kachelriess M. 2015. Evolution in computed tomography: the battle for speed and dose. *Investig. Radiol.* 50:629–44
17. Zhang J, Maniawski P, Knopp MV. 2018. Performance evaluation of the next generation solid-state digital photon counting PET/CT system. *EJNMMI Res.* 8:97
18. van Sluis JJ, de Jong J, Schaar J, Noordzij W, van Snick P, et al. 2019. Performance characteristics of the digital Biograph Vision PET/CT system. *J. Nucl. Med.* 60:1031–36
19. Pan T, Einstein SA, Kappadath SC, Grogg KS, Lois Gomez C, et al. 2019. Performance evaluation of the 5-ring GE Discovery MI PET/CT system using the National Electrical Manufacturers Association NU 2-2012 standard. *Med. Phys.* 46:3025–33
20. Surti S, Pantel AR, Karp JS. 2020. Total body PET: Why, how, what for? *IEEE Trans. Radiat. Plasma Med. Sci.* 4:283–92
21. Zhang X, Cherry SR, Xie Z, Shi H, Badawi RD, Qi J. 2020. Subsecond total-body imaging using ultrasensitive positron emission tomography. *PNAS* 117:2265–67
22. Schaart DR, Ziegler S, Zaidi H. 2020. Achieving 10 ps coincidence time resolution in TOF-PET is an impossible dream. *Med. Phys.* 47:2721–24
23. Lecoq P, Morel C, Prior J, Visvikis D, Gundacker S, et al. 2020. Roadmap toward the 10 ps time-of-flight PET challenge. *Phys. Med. Biol.* 65:21RM01

24. Zaidi H, Becker M. 2016. The promise of hybrid PET/MRI: technical advances and clinical applications. *IEEE Signal Process. Mag.* 33:67–85
25. Judenhofer MS, Wehrl HF, Newport DF, Catana C, Siegel SB, et al. 2008. Simultaneous PET-MRI: a new approach for functional and morphological imaging. *Nat. Med.* 14:459–65
26. Zaidi H, Ojha N, Morich M, Griesmer J, Hu Z, et al. 2011. Design and performance evaluation of a whole-body Ingenuity TF PET-MRI system. *Phys. Med. Biol.* 56:3091–106
27. Delso G, Fürst S, Jakoby B, Ladebeck R, Ganter C, et al. 2011. Performance measurements of the Siemens mMR integrated whole-body PET/MR scanner. *J. Nucl. Med.* 52:1914–22
28. Grant AM, Deller TW, Khalighi MM, Maramraju SH, Delso G, Levin CS. 2016. NEMA NU 2-2012 performance studies for the SiPM-based ToF-PET component of the GE SIGNA PET/MR system. *Med. Phys.* 43:2334–43
29. Veit-Haibach P, Kuhn F, Wiesinger F, Delso G, von Schulthess G. 2013. PET–MR imaging using a tri-modality PET/CT–MR system with a dedicated shuttle in clinical routine. *Magn. Reson. Mater. Phys. Biol. Med.* 26:25–35
30. Kolb A, Wehrl HF, Hofmann M, Judenhofer MS, Eriksson L, et al. 2012. Technical performance evaluation of a human brain PET/MRI system. *Eur. Radiol.* 22:1776–88
31. Cho ZH, Son YD, Kim HK, Kim KN, Oh SH, et al. 2008. A fusion PET-MRI system with a high-resolution research tomograph PET and ultra-high field 7.0 T MRI for the molecular-genetic imaging of the brain. *Proteomics* 8:1302–23
32. Liu G, Cao T, Hu L, Zheng J, Pang L, et al. 2019. Validation of MR-based attenuation correction of a newly released whole-body simultaneous PET/MR system. *Biomed. Res. Int.* 2019:8213215
33. van der Vos CS, Koopman D, Rijnsdorp S, Arends AJ, Boellaard R, et al. 2017. Quantification, improvement, and harmonization of small lesion detection with state-of-the-art PET. *Eur. J. Nucl. Med. Mol. Imaging* 44:4–16
34. Zaidi H, Karakatsanis N. 2018. Towards enhanced PET quantification in clinical oncology. *Br. J. Radiol.* 91:20170508
35. Reader AJ, Zaidi H. 2007. Advances in PET image reconstruction. *PET Clin.* 2:173–90
36. Rahmim A, Qi J, Sossi V. 2013. Resolution modeling in PET imaging: theory, practice, benefits, and pitfalls. *Med. Phys.* 40:064301
37. Yip SS, Aerts HJ. 2016. Applications and limitations of radiomics. *Phys. Med. Biol.* 61:R150–66
38. Avanzo M, Stancanello J, El Naqa I. 2017. Beyond imaging: the promise of radiomics. *Phys. Med.* 38:122–39
39. Rahmim A, Lodge MA, Karakatsanis NA, Panin VY, Zhou Y, et al. 2019. Dynamic whole-body PET imaging: principles, potentials and applications. *Eur. J. Nucl. Med. Mol. Imaging* 46:501–18
40. Zaker N, Kotasidis F, Garibotto V, Zaidi H. 2020. Assessment of lesion detectability in dynamic whole-body PET imaging using compartmental and Patlak parametric mapping. *Clin. Nucl. Med.* 45:e221–31
41. Rumelhart DE, Hinton GE, Williams RJ. 1986. Learning representations by back-propagating errors. *Nature* 323:533–36
42. Hinton GE, Salakhutdinov RR. 2006. Reducing the dimensionality of data with neural networks. *Science* 313:504–7
43. LeCun Y, Bengio Y, Hinton G. 2015. Deep learning. *Nature* 521:436–44
44. Lecun Y, Bottou L, Bengio Y, Haffner P. 1998. Gradient-based learning applied to document recognition. *Proc. IEEE* 86:2278–324
45. Goodfellow I, Bengio Y, Courville A. 2016. *Deep Learning*. Cambridge, MA: MIT Press
46. Khan A, Sohail A, Zahoora U, Qureshi AS. 2019. A survey of the recent architectures of deep convolutional neural networks. arXiv:1901.06032v7 [cs.CV]
47. Hochreiter S, Schmidhuber J. 1997. Long short-term memory. *Neural Comput.* 9:1735–80
48. Cho K, van Merrienboer B, Gulcehre C, Bahdanau D, Bougares F, et al. 2014. Learning phrase representations using RNN encoder-decoder for statistical machine translation. arXiv:1406.1078 [cs.CL]
49. Goodfellow IJ, Pouget-Abadie J, Mirza M, Xu B, Warde-Farley D, et al. 2014. Generative adversarial networks. arXiv:1406.2661 [stat.ML]

50. Liu X, Faes L, Kale AU, Wagner SK, Fu DJ, et al. 2019. A comparison of deep learning performance against health-care professionals in detecting diseases from medical imaging: a systematic review and meta-analysis. *Lancet Digit. Health* 1:e271–97
51. Gong K, Berg E, Cherry SR, Qi J. 2020. Machine learning in PET: from photon detection to quantitative image reconstruction. *Proc. IEEE* 108:51–68
52. Zaharchuk G. 2019. Next generation research applications for hybrid PET/MR and PET/CT imaging using deep learning. *Eur. J. Nucl. Med. Mol. Imaging* 46:2700–7
53. Ravishankar H, Sudhakar P, Venkataramani R, Thiruvenkadam S, Annangi P, et al. 2016. Understanding the mechanisms of deep transfer learning for medical images. In *Deep Learning and Data Labeling for Medical Applications*, ed. G Carneiro, D Mateus, P Loïc, A Bradley, JMRS Tavares, et al., pp. 188–96. Berlin: Springer
54. Wang H, Zhou Z, Li Y, Chen Z, Lu P, et al. 2017. Comparison of machine learning methods for classifying mediastinal lymph node metastasis of non-small-cell lung cancer from ^{18}F-FDG PET/CT images. *EJNMMI Res.* 7:11
55. Zhu B, Liu JZ, Cauley SF, Rosen BR, Rosen MS. 2018. Image reconstruction by domain-transform manifold learning. *Nature* 555:487–92
56. Wang Q, Liu Z, Ziegler SI, Shi K. 2015. Enhancing spatial resolution of ^{18}F positron imaging with the Timepix detector by classification of primary fired pixels using support vector machine. *Phys. Med. Biol.* 60:5261–78
57. Sanaat A, Zaidi H. 2020. Depth of interaction estimation in a preclinical PET scanner equipped with monolithic crystals coupled to SiPMs using a deep neural network. *Appl. Sci.* 10:4753
58. Berg E, Cherry SR. 2018. Using convolutional neural networks to estimate time-of-flight from PET detector waveforms. *Phys. Med. Biol.* 63:02LT1
59. Whiteley W, Gregor J. 2019. CNN-based PET sinogram repair to mitigate defective block detectors. *Phys. Med. Biol.* 64:235017
60. Häggström I, Schmidtlein CR, Campanella G, Fuchs TJ. 2019. DeepPET: a deep encoder–decoder network for directly solving the PET image reconstruction inverse problem. *Med. Image Anal.* 54:253–62
61. Reader AJ, Corda G, Mehranian A, da Costa-Luis C, Ellis S, Schnabel JA. 2021. Deep learning for PET image reconstruction. *IEEE Trans. Radiat. Plasma Med. Sci.* 5:1–25
62. Gong K, Guan J, Kim K, Zhang X, Yang J, et al. 2019. Iterative PET image reconstruction using convolutional neural network representation. *IEEE Trans. Med. Imaging* 38:675–85
63. Mehranian A, Reader AJ. 2021. Model-based deep learning PET image reconstruction using forward-backward splitting expectation maximisation. *IEEE Trans. Radiat. Plasma Med. Sci.* 5:54–64
64. Mehranian A, Arabi H, Zaidi H. 2016. Vision 20/20: magnetic resonance imaging–guided attenuation correction in PET/MRI: challenges, solutions, and opportunities. *Med. Phys.* 43:1130–55
65. Arabi H, Zeng G, Zheng G, Zaidi H. 2019. Novel adversarial semantic structure deep learning for MRI-guided attenuation correction in brain PET/MRI. *Eur. J. Nucl. Med. Mol. Imaging* 46:2746–59
66. Liu F, Jang H, Kijowski R, Bradshaw T, McMillan AB. 2018. Deep learning MR imaging–based attenuation correction for PET/MR imaging. *Radiology* 286:676–84
67. Leynes AP, Yang J, Wiesinger F, Kaushik SS, Shanbhag DD, et al. 2018. Zero-echo-time and Dixon deep pseudo-CT (ZeDD CT): direct generation of pseudo-CT images for pelvic PET/MRI attenuation correction using deep convolutional neural networks with multiparametric MRI. *J. Nucl. Med.* 58:852–58
68. Hwang D, Kang SK, Kim KY, Seo S, Paeng JC, et al. 2019. Generation of PET attenuation map for whole-body time-of-flight ^{18}F-FDG PET/MRI using a deep neural network trained with simultaneously reconstructed activity and attenuation maps. *J. Nucl. Med.* 60:1183–89
69. Torrado-Carvajal A, Vera-Olmos J, Izquierdo-Garcia D, Catalano OA, Morales MA, et al. 2019. Dixon-VIBE deep learning (DIVIDE) pseudo-CT synthesis for pelvis PET/MR attenuation correction. *J. Nucl. Med.* 60:429–35
70. Pozaruk A, Pawar K, Li S, Carey A, Cheng J, et al. 2021. Augmented deep learning model for improved quantitative accuracy of MR-based PET attenuation correction in PSMA PET-MRI prostate imaging. *Eur. J. Nucl. Med. Mol. Imaging* 41:9–20

71. Ladefoged CN, Hansen AE, Henriksen OM, Bruun FJ, Eikenes L, et al. 2020. AI-driven attenuation correction for brain PET/MRI: clinical evaluation of a dementia cohort and importance of the training group size. *NeuroImage* 222:117221
72. Mostafapour S, Gholamiankhah F, Dadgar H, Arabi H, Zaidi H. 2021. Feasibility of deep learning–guided attenuation and scatter correction of whole-body ^{68}Ga-PSMA PET studies in the image domain. *Clin. Nucl. Med*. In press. **https://doi.org/10.1097/RLU.0000000000003585**
73. Arabi H, Koutsouvelis N, Rouzaud M, Miralbell R, Zaidi H. 2016. Atlas-guided generation of pseudo-CT images for MRI-only and hybrid PET-MRI-guided radiotherapy treatment planning. *Phys. Med. Biol.* 61:6531–52
74. Arabi H, Zaidi H. 2020. Truncation compensation and metallic dental implant artefact reduction in PET/MRI attenuation correction using deep learning–based object completion. *Phys. Med. Biol.* 65:195002
75. Zaidi H, Koral KF. 2004. Scatter modelling and compensation in emission tomography. *Eur. J. Nucl. Med. Mol. Imaging* 31:761–82
76. Xiang H, Lim H, Fessler JA, Dewaraja YK. 2020. A deep neural network for fast and accurate scatter estimation in quantitative SPECT/CT under challenging scatter conditions. *Eur. J. Nucl. Med. Mol. Imaging* 47:2956–67
77. Yang J, Park D, Gullberg GT, Seo Y. 2019. Joint correction of attenuation and scatter in image space using deep convolutional neural networks for dedicated brain ^{18}F-FDG PET. *Phys. Med. Biol.* 64:075019
78. Shiri I, Ghafarian P, Geramifar P, Leung KH, Ghelichoghli M, et al. 2019. Direct attenuation correction of brain PET images using only emission data via a deep convolutional encoder–decoder (Deep-DAC). *Eur. Radiol.* 29:6867–79
79. Dong X, Lei Y, Wang T, Higgins K, Liu T, et al. 2020. Deep learning–based attenuation correction in the absence of structural information for whole-body PET imaging. *Phys. Med. Biol.* 65:055011
80. Shiri I, Arabi H, Geramifar P, Hajianfar G, Ghafarian P, et al. 2020. Deep-JASC: joint attenuation and scatter correction in whole-body ^{18}F-FDG PET using a deep residual network. *Eur. J. Nucl. Med. Mol. Imaging* 47:2533–48
81. Arabi H, Bortolin K, Ginovart N, Garibotto V, Zaidi H. 2020. Deep learning–guided joint attenuation and scatter correction in multitracer neuroimaging studies. *Hum. Brain Mapp.* 41:3667–79
82. Pham DL, Xu C, Prince JL. 2000. Current methods in medical image segmentation. *Annu. Rev. Biomed. Eng.* 2:315–37
83. Seo H, Badiei Khuzani M, Vasudevan V, Huang C, Ren H, et al. 2020. Machine learning techniques for biomedical image segmentation: an overview of technical aspects and introduction to state-of-art applications. *Med. Phys.* 47:e148–67
84. Zaidi H, Xu XG. 2007. Computational anthropomorphic models of the human anatomy: the path to realistic Monte Carlo modeling in medical imaging. *Annu. Rev. Biomed. Eng.* 9:471–500
85. Hatt M, Lee J, Schmidtlein CR, El Naqa I, Caldwell C, et al. 2017. Classification and evaluation strategies of auto-segmentation approaches for PET: report of AAPM Task Group no. 211. *Med. Phys.* 44:e1–42
86. Xie T, Zaidi H. 2019. Estimation of the radiation dose in pregnancy: an automated patient-specific model using convolutional neural networks. *Eur. Radiol.* 29:6805–15
87. Chen L, Shen C, Zhou Z, Maquilan G, Albuquerque K, et al. 2019. Automatic PET cervical tumor segmentation by combining deep learning and anatomic prior. *Phys. Med. Biol.* 64:085019
88. Li L, Zhao X, Lu W, Tan S. 2020. Deep learning for variational multimodality tumor segmentation in PET/CT. *Neurocomputing* 392:277–95
89. Blanc-Durand P, Van Der Gucht A, Schaefer N, Itti E, Prior JO. 2018. Automatic lesion detection and segmentation of ^{18}F-FET PET in gliomas: a full 3D U-Net convolutional neural network study. *PLOS ONE* 13:e0195798
90. Lu Y, Lin J, Chen S, He H, Cai Y. 2020. Automatic tumor segmentation by means of deep convolutional U-Net with pre-trained encoder in PET images. *IEEE Access*. 8:113636–48
91. Arabi H, Shiri I, Janebi E, Becker M, Zaidi H. 2020. *Deep learning–based automated delineation of head and neck malignant lesions from PET images*. Paper presented at IEEE Nuclear Science Symposium and Medical Imaging Conference (NSS/MIC), online, Oct. 31–Nov. 7

92. Fu Y, Lei Y, Wang T, Curran WJ, Liu T, Yang X. 2020. Deep learning in medical image registration: a review. *Phys. Med. Biol.* 65:20TR01
93. de Vos BD, Berendsen FF, Viergever MA, Sokooti H, Staring M, Isgum I. 2019. A deep learning framework for unsupervised affine and deformable image registration. *Med. Image Anal.* 52:128–43
94. Li T, Zhang M, Qi W, Asma E, Qi J. 2020. Motion correction of respiratory-gated PET images using deep learning based image registration framework. *Phys. Med. Biol.* 65:155003
95. Wang Y, Yu B, Wang L, Zu C, Lalush DS, et al. 2018. 3D conditional generative adversarial networks for high-quality PET image estimation at low dose. *NeuroImage* 174:550–62
96. Ouyang J, Chen KT, Gong E, Pauly J, Zaharchuk G. 2019. Ultra-low-dose PET reconstruction using generative adversarial network with feature matching and task-specific perceptual loss. *Med. Phys.* 46:3555–64
97. Chen KT, Gong E, de Carvalho Macruz FB, Xu J, Boumis A, et al. 2019. Ultra-low-dose ^{18}F-florbetaben amyloid PET imaging using deep learning with multi-contrast MRI inputs. *Radiology* 290:649–56
98. Kaplan S, Zhu Y-M. 2019. Full-dose PET image estimation from low-dose PET image using deep learning: a pilot study. *J. Digit. Imaging* 32:773–78
99. Zhou L, Schaefferkoetter JD, Tham IWK, Huang G, Yan J. 2020. Supervised learning with cyclegan for low-dose FDG PET image denoising. *Med. Image Anal.* 65:101770
100. Sanaat A, Arabi H, Mainta I, Garibotto V, Zaidi H. 2020. Projection-space implementation of deep learning–guided low-dose brain PET imaging improves performance over implementation in image-space. *J. Nucl. Med.* 61:1388–96
101. Cui J, Gong K, Guo N, Wu C, Meng X, et al. 2019. PET image denoising using unsupervised deep learning. *Eur. J. Nucl. Med. Mol. Imaging* 46:2780–89
102. Lu W, Onofrey JA, Lu Y, Shi L, Ma T, et al. 2019. An investigation of quantitative accuracy for deep learning based denoising in oncological PET. *Phys. Med. Biol.* 64:165019
103. Gong K, Guan J, Liu C, Qi J. 2019. PET image denoising using a deep neural network through fine tuning. *IEEE Trans. Radiat. Plasma Med. Sci.* 3:153–61
104. Lei Y, Dong X, Wang T, Higgins K, Liu T, et al. 2019. Whole-body PET estimation from low count statistics using cycle-consistent generative adversarial networks. *Phys. Med. Biol.* 64:215017
105. Lei Y, Wang T, Dong X, Higgins K, Liu T, et al. 2020. Low dose PET imaging with CT-aided cycle-consistent adversarial networks. *Proc. SPIE* 11312:1131247
106. Sanaat A, Shiri I, Arabi H, Mainta I, Nkoulou R, Zaidi H. 2020. *Whole-body PET image synthesis from low-dose images using cycle-consistent generative adversarial networks*. Paper presented at IEEE Nuclear Science Symposium and Medical Imaging Conference (NSS/MIC), online, Oct. 31–Nov. 7
107. Shiri I, AmirMozafari Sabet K, Arabi H, Pourkeshavarz M, Teimourian B, et al. 2020. Standard SPECT myocardial perfusion estimation from half-time acquisitions using deep convolutional residual neural networks. *J. Nucl. Cardiol.* **https://doi.org/10.1007/s12350-020-02119-y**
108. Ramon AJ, Yang Y, Pretorius PH, Johnson KL, King MA, Wernick MN. 2020. Improving diagnostic accuracy in low-dose SPECT myocardial perfusion imaging with convolutional denoising networks. *IEEE Trans. Med. Imaging* 39:2893–903
109. Song T-A, Chowdhury SR, Yang F, Dutta J. 2020. PET image super-resolution using generative adversarial networks. *Neural Netw.* 125:83–91
110. Nguyen D, Long T, Jia X, Lu W, Gu X, et al. 2019. A feasibility study for predicting optimal radiation therapy dose distributions of prostate cancer patients from patient anatomy using deep learning. *Sci. Rep.* 9:1076
111. Xing Y, Zhang Y, Nguyen D, Lin M-H, Lu W, Jiang S. 2020. Boosting radiotherapy dose calculation accuracy with deep learning. *J. Appl. Clin. Med. Phys.* 21:149–59
112. Mao X, Pineau J, Keyes R, Enger SA. 2020. RapidBrachyDL: rapid radiation dose calculations in brachytherapy via deep learning. *Int. J. Radiat. Oncol. Biol. Phys.* 108:802–12
113. Lee MS, Hwang D, Kim JH, Lee JS. 2019. Deep-dose: a voxel dose estimation method using deep convolutional neural network for personalized internal dosimetry. *Sci. Rep.* 9:10308
114. Götz TI, Schmidkonz C, Chen S, Al-Baddai S, Kuwert T, Lang EW. 2020. A deep learning approach to radiation dose estimation. *Phys. Med. Biol.* 65:035007

115. Akhavanallaf A, Shiri I, Arabi H, Zaidi H. 2020. Whole-body voxel-based internal dosimetry using deep learning. *Eur. J. Nucl. Med. Mol. Imaging.* **https://doi.org/10.1007/s00259-020-05013-4**
116. Ding Y, Sohn JH, Kawczynski MG, Trivedi H, Harnish R, et al. 2019. A deep learning model to predict a diagnosis of Alzheimer disease by using ^{18}F-FDG PET of the brain. *Radiology* 290:456–64
117. Sibille L, Seifert R, Avramovic N, Vehren T, Spottiswoode B, et al. 2019. ^{18}F-FDG PET/CT uptake classification in lymphoma and lung cancer by using deep convolutional neural networks. *Radiology* 294:191114
118. Avanzo M, Wei L, Stancanello J, Vallieres M, Rao A, et al. 2020. Machine and deep learning methods for radiomics. *Med. Phys.* 47:e185–202
119. Zaidi H, Alavi A, El Naqa I. 2018. Novel quantitative PET techniques for clinical decision support in oncology. *Semin. Nucl. Med.* 48:548–64
120. Papp L, Poetsch N, Grahovac M, Schmidbauer V, Woehrer A, et al. 2018. Glioma survival prediction with the combined analysis of in vivo ^{11}C-MET-PET, ex vivo and patient features by supervised machine learning. *J. Nucl. Med.* 59:892–99
121. Waninger JJ, Green MD, Cheze Le Rest C, Rosen B, El Naqa I. 2019. Integrating radiomics into clinical trial design. *Q. J. Nucl. Med. Mol. Imaging* 63:339–46
122. Li Z, Wang Y, Yu J, Guo Y, Cao W. 2017. Deep learning based radiomics (DLR) and its usage in non-invasive IDH1 prediction for low grade glioma. *Sci. Rep.* 7:5467
123. Wei L, Osman S, Hatt M, El Naqa I. 2019. Machine learning for radiomics-based multimodality and multiparametric modeling. *Q. J. Nucl. Med. Mol. Imaging* 63:323–38
124. Shiri I, Maleki H, Hajianfar G, Abdollahi H, Ashrafinia S, et al. 2020. Next-generation radiogenomics sequencing for prediction of EGFR and KRAS mutation status in NSCLC patients using multimodal imaging and machine learning algorithms. *Mol. Imaging Biol.* 22:1132–48
125. Hutson M. 2018. Artificial intelligence faces reproducibility crisis. *Science* 359:725–26
126. Carter RE, Attia ZI, Lopez-Jimenez F, Friedman PA. 2019. Pragmatic considerations for fostering reproducible research in artificial intelligence. *npj Digit. Med.* 2:42
127. Prior F, Smith K, Sharma A, Kirby J, Tarbox L, et al. 2017. The public cancer radiology imaging collections of the Cancer Imaging Archive. *Sci. Data* 4:170124
128. Hatt M, Laurent B, Ouahabi A, Fayad H, Tan S, et al. 2018. The first MICCAI challenge on PET tumor segmentation. *Med. Image Anal.* 44:177–95
129. Andrearczyk V, Oreiller V, Jreige M, Vallières M, Castelli J, et al. 2021. Overview of the HECKTOR Challenge at MICCAI 2020: automatic head and neck tumor segmentation in PET/CT. In *Head and Neck Tumor Segmentation: HECKTOR 2020*, ed. V Andrearczyk, V Oreiller, A Depeursinge, pp. 1–21. Cham, Switz.: Springer
130. Elhalawani H. 2018. *^{18}F-FDG PET risk stratifiers in head and neck cancer: a MICCAI 2018 CPM Grand Challenge*. Grand Challenge Overview, MICCAI, Granada, Spain. **https://www.kaggle.com/c/pet-radiomics-challenges** Accessed February 2021
131. Dewaraja Y, Frey E, Sunderland J, Uribe C. 2021. *^{177}Lu dosimetry challenge of the SNMMI Dosimetry Task Force*. Grand Challenge Overview, SNMMI, Reston, VA. **https://therapy.snmmi.org/SNMMI-THERAPY/Dosimetry_Challenge.aspx**
132. Armato SG 3rd, Farahani K, Zaidi H. 2020. Biomedical image analysis challenges should be considered as an academic exercise, not an instrument that will move the field forward in a real, practical way. *Med. Phys.* 47:2325–28
133. Maier-Hein L, Eisenmann M, Reinke A, Onogur S, Stankovic M, et al. 2018. Why rankings of biomedical image analysis competitions should be interpreted with care. *Nat. Commun.* 9:5217
134. Kagadis GC, Kloukinas C, Moore K, Philbin J, Papadimitroulas P, et al. 2013. Cloud computing in medical imaging. *Med. Phys.* 40:070901
135. Guinney J, Saez-Rodriguez J. 2018. Alternative models for sharing confidential biomedical data. *Nat. Biotechnol.* 36:391–92
136. Castro DC, Walker I, Glocker B. 2020. Causality matters in medical imaging. *Nat. Commun.* 11:3673
137. Cui S, Tseng HH, Pakela J, Ten Haken RK, El Naqa I. 2020. Introduction to machine and deep learning for medical physicists. *Med. Phys.* 47:e127–47

138. Cherkassky VS, Mulier F. 2007. *Learning from Data: Concepts, Theory, and Methods*. Hoboken, NJ: Wiley Intersci.
139. El Naqa I, Ruan D, Valdes G, Dekker A, McNutt T, et al. 2018. Machine learning and modeling: data, validation, communication challenges. *Med. Phys.* 45:e834–40
140. Collins GS, Reitsma JB, Altman DG, Moons KM. 2015. Transparent reporting of a multivariable prediction model for individual prognosis or diagnosis (TRIPOD): the TRIPOD Statement. *Ann. Intern. Med.* 162:55–63
141. Luo Y, Tseng H-H, Cui S, Wei L, Haken RKT, El Naqa I. 2019. Balancing accuracy and interpretability of machine learning approaches for radiation treatment outcomes modeling. *BJR|Open* 1:20190021
142. Philbrick KA, Yoshida K, Inoue D, Akkus Z, Kline TL, et al. 2018. What does deep learning see? Insights from a classifier trained to predict contrast enhancement phase from CT images. *Am. J. Roentgenol.* 211:1184–93
143. Seah JCY, Tang JSN, Kitchen A, Gaillard F, Dixon AF. 2019. Chest radiographs in congestive heart failure: visualizing neural network learning. *Radiology* 290:514–22
144. Luna JM, Gennatas ED, Ungar LH, Eaton E, Diffenderfer ES, et al. 2019. Building more accurate decision trees with the additive tree. *PNAS* 116:19887–93
145. Nazmul Haque K, Latif S, Rana R. 2019. Disentangled representation learning with information maximizing autoencoder. arXiv:1904.08613 [cs.LG]
146. Maier AK, Syben C, Stimpel B, Würfl T, Hoffmann M, et al. 2019. Learning with known operators reduces maximum error bounds. *Nat. Mach. Intell.* 1:373–80
147. Cova TFGG, Bento DJ, Nunes SCC. 2019. Computational approaches in theranostics: mining and predicting cancer data. *Pharmaceutics* 11:119
148. Liu CC, Huang HM. 2019. Partial-ring PET image restoration using a deep learning based method. *Phys. Med. Biol.* 64:225014